Axisymmetric Density Field Measurements by Moire Deflectometry

J. Stricker*
Technion—Israel Institute of Technology, Haifa, Israel
and
E. Keren† and O. Kafri†
Nuclear Research Center, Beer-Sheva, Israel

Introduction

A NEW noncoherent method for studying phase objects, moire deflectometry,[1] has been applied successfully for mapping the density field of a two-dimensional flow past a diamond airfoil in a supersonic wind tunnel.[2] There the density was constant along the lines perpendicular to the flow direction, and the interpretation of the resulting deflectogram was straightforward. In the present Note we extend the method to flow patterns having axial symmetry.

Experimental

The setup is similar to that of Ref. 2. Two Ronchi rulings, G_1 and G_2, having a pitch p were set a distance Δ apart and oriented at angles $+\theta/2$ and $-\theta/2$, respectively, relative to the z axis. When a parallel collimated beam passes through the gratings, a moire pattern is produced on a mat screen attached to G_2. The pattern consists of straight fringes parallel to the y axis separated by a distance p'

$$p' = \frac{p}{2\sin(\theta/2)} \tag{1}$$

When the beam passes through the flowfield it is disturbed due to density gradients and the moire pattern is deformed. The calculation of the beam deflection angles (from the fringe distortion) makes possible the determination of the index of refraction gradients along the optical path.

The model tested was a circular cone with cone angle of 23 deg, held at a zero angle of attack in the wind tunnel. Under these circumstances an axisymmetric flowfield is established past the cone. The Mach number was 1.98, the stagnation pressure $p_{st} = 3.15$ atm, and the static pressure was 0.415 atm. The moire pattern (Fig. 1) shows clearly the conical shock wave emerging from the apex and the expansion fans centered on the shoulders. The geometry of the experiment is shown in Fig. 2.

Analysis and Results

The flow past the cone is compressed by an oblique conical shock wave and remains constant on cones having a common vertex. Between the shock wave and the cone surface the flow conditions vary, as shown by the calculated curve in Fig. 3. The values of the density at the cone surface and shock wave were taken from Ref. 3. The variation of density between those boundaries was obtained by numerical integration of the flow equations, as suggested by Taylor and Maccoll.[4] These calculations will be compared to the density profiles evaluated from the deflectogram of Fig. 1.

The component of the deflection to the y direction of a light ray traveling along the x direction through a continuous phase object is

$$\tan\varphi \simeq \varphi(y,z) = \frac{1}{n_\infty}\int_{-\infty}^{\infty} \frac{\partial n(x,y,z)}{\partial y}\,dx \tag{2}$$

where $n(x,y,z)$ and n_∞ are the index of refraction of the object and the surroundings, respectively, and the paraxial approximation has been used in deriving the equation. For an object of axial symmetry $n(x,y,z) = n(r,z)$ $[r = (x^2+y^2)^{1/2}]$, and Eq. (2) is transformed to

$$\varphi(y,z) = 2y\int_y^{r_s(z)} \frac{\partial n(r,z)}{\partial r}\frac{dr}{(r^2-y^2)^{1/2}} \tag{3}$$

where the upper bound has been replaced by $r_s(z)$, the radius of the shock wave, since $n(r,z)$ is equal to n_∞ at $r > r_s$. If n is constant on cones having a common vertex at the apex of the object then $n(r,z) = n(a)$ where $a \equiv \tan\alpha = r/z$ and α is the angle of that particular cone. Substituting a into Eq. (3) we get

$$\varphi(y,z) = \varphi(b) = 2b\int_b^{a_s} \frac{\partial n}{\partial a}\frac{da}{(a^2-b^2)^{1/2}} \tag{4}$$

where $a_s = \tan(\alpha_s) = r_s(z)/z$ and $b = \tan(\beta) = y/z$.

Let $z(y)$ be the functional form of a particular fringe and $h(y,z) = z(y) - z(0)$ is the deviation of that fringe from its unperturbed position. Inspection of Fig. 1 shows that $h(y,z)$ may be approximated by straight lines in the region between the shock and the head of the expansion fan,

$$h(y,z) = \frac{dh}{dy}y = \frac{dz}{dy}y \qquad y \le r_s \tag{5}$$

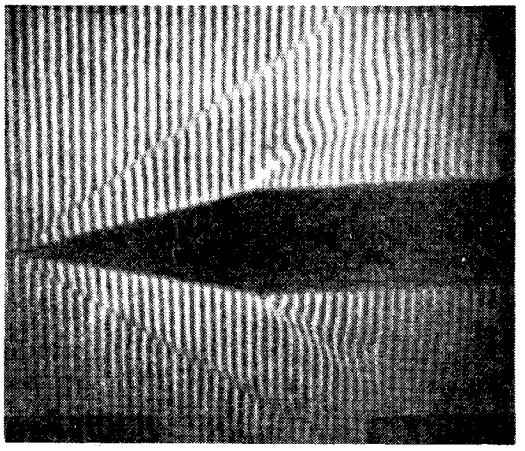

Fig. 1 Deflectogram of a 23 deg circular cone in the supersonic wind tunnel at a zero angle of attack. Flow conditions: $M = 1.98$, $p_{st} = 3.15$ atm.

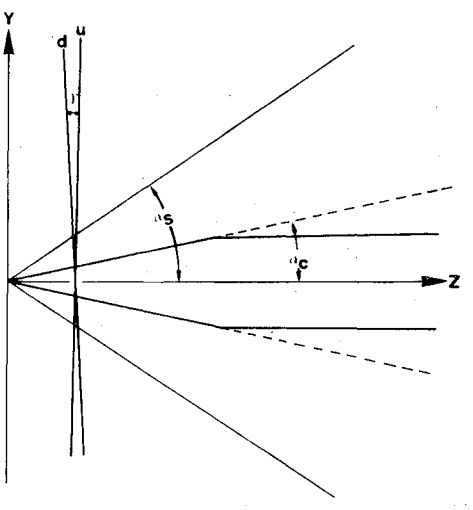

Fig. 2 Geometry of the experiment. α_c and α_s are the cone angles of the object and shock front, respectively. *u* denotes an unperturbed fringe, and *d* denotes the corresponding disturbed fringe.

Received June 21, 1982; revision received Feb. 28, 1983. Copyright © 1983 by J. Stricker. Published by the American Institute of Aeronautics and Astronautics with permission.

*Senior Lecturer, Department of Aeronautical Engineering.
†Senior Research Scientist.

The slope dz/dy of a representative fringe is shown in Fig. 2. When the angle θ between the gratings is small, the deflection angle φ is given in terms of h by[1,2]:

$$\varphi(y,z) = (\theta/\Delta)h(y,z) \tag{6}$$

thus, if φ satisfies Eq. (4), $h(y,z)$ must also be a function of $b=y/z$, and Eq. (5) means that dy/dz is proportional to z

$$\frac{dy}{dz} = -\frac{z}{k} \tag{7}$$

$$h(y,z) = -kb \tag{8}$$

where k is a constant. To test this conclusion we plotted the slopes dy/dz of the various fringes vs the corresponding $z \doteq z(0)$ positions (Fig. 4). Within the experimental scatter, the result is a straight line passing through the origin. A least-square calculation produced a value for the constant $k=1.32\pm0.05$ mm. Thus the linear result supports the theoretical prediction of constant index of refraction on cones whose apex coincides with the origin. From Eqs. (6) and (8) and the small angle limit of Eq. (1) we get an explicit expression for φ

$$\varphi(b) = -kpb/\Delta p' \qquad b \le a_s \tag{9}$$

The inverse of Eq. (4) is[5]:

$$\Delta n(a) = n_a - n_\infty = \frac{-1}{\pi}\int_a^{a_s} \frac{\varphi(b)\,db}{(b^2-a^2)^{1/2}} \tag{10}$$

Substituting Eq. (9) into Eq. (10) gives an expression for the index of refraction profile

$$\Delta n(a) = 1/\pi\,(k/p')\,(p/\Delta)\,(a_s^2-a^2)^{1/2} \tag{11}$$

and is plotted in Fig. 3 as $\Delta\rho$ vs a, where $\Delta\rho/\Delta n = 4.4$ g/cm^3 (Ref. 2). The values of the parameters used are: $p=0.308$ mm, $\Delta=726$ mm (both measured in the experimental setup), $k=1.32$ mm; and $p'=2.2$ mm (measured on the original photograph of Fig. 1, since they appear as k/p' they need not be rescaled to the actual dimensions of the experiment and the enlargement factor of the photographic process is irrelevant).

The difference between the theoretical and experimental curves is within the error bounds, except close to the shock wave angle α_s. This discrepancy results from the choice of a linear fringe shape all the way up to the shock front, which is unable to reproduce the discontinuity in density across the shock wave. However, this result is of value since it shows that the entire density distribution can be fitted reasonably well with a single measured parameter. The contribution of the discontinuity will be evaluated now.

A step function refractive index of the form

$$\Delta n(a) = \Delta n_s[1-\theta(a-a_s)] \tag{12}$$

with the derivative

$$\partial n/\partial a = -\Delta n_s \delta(a-a_s)$$

produces the following result when combined with Eq. (4) (with the upper bound equal to infinity):

$$\phi(b) = -2b\Delta n_s/[(a_s^2-b^2)^{1/2}] \tag{13}$$

This procedure is equivalent to the application of Snells law (in the paraxial approximation) at the two crossings of the shock front. The Snell law does not diverge at $b\to a_s$; however, $\tan\phi(a_s)$ is several orders of magnitude higher than typical measurable values, and, therefore, it is practically infinite [cf. Eq. (2)]. By fitting the deviation of the fringes from linearity

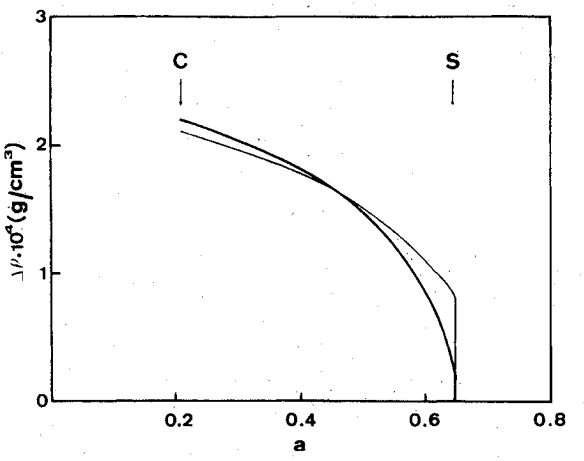

Fig. 3 Variation of the density $\Delta\rho=\rho(a)-\rho(\infty)$ vs a, the tangent of the coordinate angle α. α_c and α_s denote the cone angles of the object and the shock wave, respectively. The thin line and the thick line represent the theoretical and experimental results, respectively.

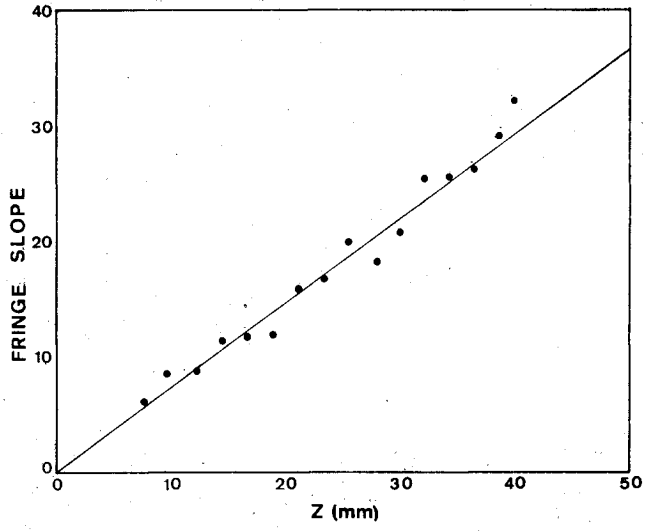

Fig. 4 The slope dy/dz of the distorted fringes vs the coordinate z of the corresponding undisturbed fringes.

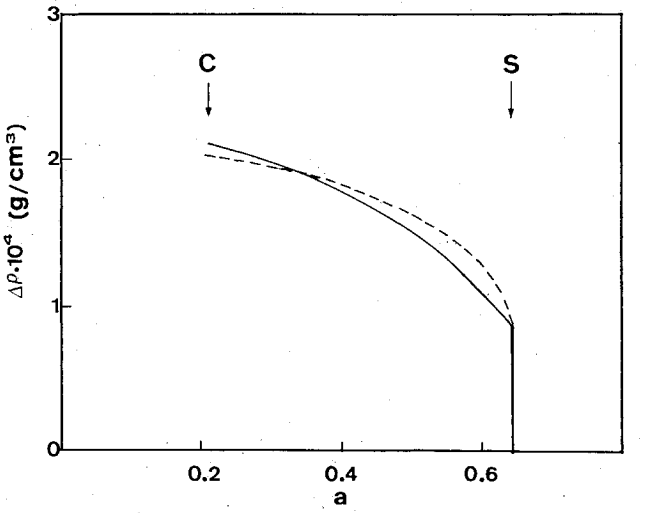

Fig. 5 Dashed line, density calculated from Eq. (6); solid line, theoretical calculation, as in Fig. 3.

near the shock front to the functional form of Eq. (13), the value $\Delta n_s = (1.9 \pm 0.2) \times 10^{-5}$ was obtained for the jump in refractive index across the shock.

Combining the contribution of the bulk [Eq. (9)] with that of the boundary [Eq. (13)] we get:

$$\phi(b) = -\left[\frac{k'p}{p'\Delta} + \frac{2\Delta n_s}{(a_s^2 - b^2)^{1/2}}\right] b \tag{14}$$

The revised constant k' is calculated by equating the small b limit of Eq. (14) with the linear approximation [Eq. (9)]

$$\frac{k'p}{p'\Delta} + \frac{2\Delta n_s}{a_s} = \frac{kp}{p'\Delta}$$

$$k' = k - (2\Delta n_s p'\Delta / p a_s) = 1.02 \pm 0.07 \text{ mm} \tag{15}$$

The final refractive index distribution plotted in Fig. 5 as $\Delta\rho$ is given by

$$\Delta n(a) = \Delta n_s + \frac{1}{\pi}\frac{k'}{p'}\frac{p}{\Delta}(a_s^2 - a^2)^{1/2} \tag{16}$$

The experimental error in density of $\pm 1 \times 10^{-5}$ g/cm^3 is due mainly to the uncertainty in Δn_s.

Summary

In the present Note we demonstrate the application of moire deflectometry to the analysis of axisymmetric flows. It is shown that by evaluation of only two parameters from a deflectogram it is possible to map, with an accuracy of about 10%, the whole density field pattern in conical flows. Good agreement between the experimental and theoretical results was observed.

References

[1] Kafri, O., "Noncoherent Method for Mapping Phase Objects," *Optics Letters*, Vol. 5, Dec. 1980, pp. 555-557.

[2] Stricker, J. and Kafri, O., "Moire Deflectometry, a New Method for Density Gradient Measurements in Compressible Flows," *AIAA Journal*, Vol. 20, March 1982.

[3] "Equations, Tables and Charts for Compressible Flow," NACA Rept. 1135, 1953.

[4] Shapiro, A. H., *The Dynamics and Thermodynamics of Compressible Fluid Flow*, Part II, The Ronald Press, N.Y., 1953; also, Taylor, G. I. and Maccoll, J. W., *Proceedings of the Royal Society*, Series A, Vol. 139, 1933, p. 278.

[5] Keren, E., Bar-Ziv, E., Glatt, I., and Kafri, O., "Measurements of Temperature Distribution of Flames by Moire Deflectometry," *Applied Optics*, Vol. 20, Dec. 1981, pp. 4263-4266.

Inlet Flow Distortion in Turbomachinery: Comparison of Theory and Experiment in a Transonic Fan Stage

B. S. Seidel* and M. D. Matwey†
University of Delaware, Newark, Delaware

BOTH velocity and temperature circumferential inlet distortions are considered at upstream infinity.[5] The blade rows (Fig. 1) are modeled as semiactuator disks. Losses and quasisteady deviation angle correlations are included in the analysis. Some of the earlier papers in this area may be found in Refs. 1, 3, and 4.

The governing equations were linearized, and the perturbations in stagnation pressure and stagnation temperature (p_0 and T_0, respectively) at upstream infinity (station 1) were represented as Fourier series. The flow in the rotor is modeled as inviscid, one dimensional, compressible, and unsteady. Elsewhere the flow is steady. The deviation angles for the rotor and stator are taken to be functions of the relative inlet angle and Mach number and the correlations in Ref. 6 are used. The losses in relative stagnation pressure in the rotor and stator are assumed to occur across the trailing edge and, again, correlations from Ref. 6 were incorporated in the analysis.

Boundary conditions applied at the various stations (Fig. 1) supply the equations which permit one to solve for the several quantities introduced in the linearization of the governing equations. When the mean relative Mach number at station 2, M_2^{REL}, was greater than 1, the flow there was modeled as shown in Fig. 2.

The bow wave distance is then taken to be a function of β_2 and M_2^{REL}, as in Ref. 7. In either case, $M_2^{REL} < 1$ or $M_2^{REL} > 1$, the boundary conditions supply the linear algebraic equations for the perturbation quantities.

Results

Transonic Fan Stage

In Ref. 2, experimental data on a transonic fan stage with circumferential inlet flow distortion is given. The measurements taken at 45% from the lip, 100% design speed, and maximum mass flow are used in the following comparison with theory.

In the calculations for the theory, an effective rotor passage length of

$$\xi_{\text{eff}} = \xi_R - (s\sin\theta_1 - \bar{L})$$

was taken, where $\bar{L}$ is the standoff distance, s blade spacing, θ_1 the rotor stagger angle, and ξ_R rotor chord length. When the theory is specialized to an actuator disk, station 2A (downstream of the Prandtl-Meyer expansion) is taken out, as well as all mention of $\dot{L}$ (rate of change of standoff distance).

Figure 3 shows the distortion in stagnation pressure imposed on the stage and Fig. 4 shows the stagnation pressure perturbation at station 5, theory (calculated in two ways) and experiment. To a large extent, the experimental curve lies between the two computations for the theory. The theory is for hub-tip ratios near unity and a shock in each blade passage extending from root-to-tip. In the experiment, the hub-tip ratio is <1; there is a shock in each passage but these shocks do not extend from root-to-tip. The curves were computed using 18 harmonics. The theory shows, that for transonic

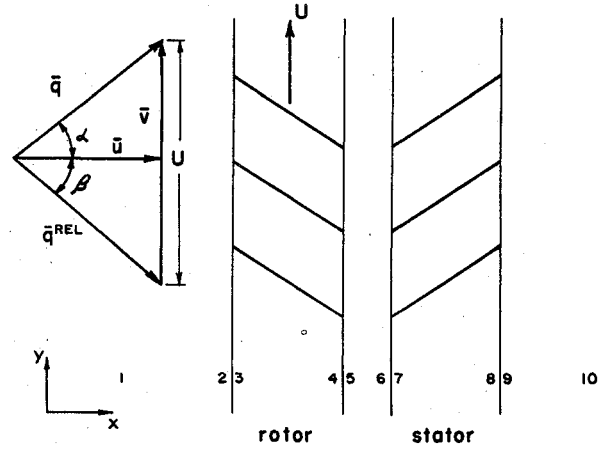

Fig. 1 Coordinates and notation.

Received July 27, 1981; revision received Feb. 23, 1983. This paper is declared a work of the U.S. Government and therefore is in the public domain.

*Professor, Department of Mechanical and Aerospace Engineering.
†Graduate Student.